Monitoring Seasonal River Ice Dynamics at the Yukon-Tanana Confluence Using Sentinel-1 SAR Data

Justin Baker

1.Introduction

The confluence of the Yukon River and the Tanana River in interior Alaska is part of a dynamic river environment containing pronounced seasonal freeze-thaw processes. These types of processes are influenced by temperature, flow conditions, and tributary inputs, and at major confluences, they can become especially complex. In addition to their environmental significance, these two rivers are critically important for supporting remote communities by providing a cost-effective transportation alternative in the absence of road networks. Therefore, monitoring river ice conditions in this region is essential for maintaining regional connectivity and resource delivery.

Given these challenges, satellite remote sensing provides an ideal approach for observing river ice dynamics. Sentinel-1, a sun-synchronous, polar-orbiting satellite constellation, utilizes synthetic aperture radar (SAR) to provide frequent and reliable radar imaging capabilities independent of cloud cover and lighting conditions. These capabilities make SAR an ideal choice for monitoring ice coverage of arctic and sub-arctic water bodies in environments where traditional optical imagery is often limited. In this analysis, Sentinel-1 data were leveraged to conduct a time series analysis of river ice dynamics at the confluence of the Yukon and Tanana Rivers in order to better understand the following:

1. Patterns in seasonal ice formation
2. How ice formation varies across years

2. Methods

2.1 Study Area

The study area encompasses the Yukon-Tanana confluence, which is located in central Alaska approximately 200 km west of Fairbanks. This area is characterized by intermontane boreal forests, which experience a fairly dry climate where forest fires are not uncommon during summer droughts. This area is also known for extreme seasonal temperature changes that include long, cold winters and short, temperate summers. The confluence represents a dynamic

river environment affected by tributary inputs, which heavily influence the formation and breakup of river ice.

2.2 Data Source

The Sentinel-1 constellation consists of two sun-synchronous polar-orbiting satellites, which perform C-band synthetic aperture radar (SAR) imaging with very short revisit times. SAR data was acquired for the months September through May spanning three consecutive winter seasons, 2022/2023, 2023/2024, and 2024/2025. All data were accessed and preprocessed using the Sentinel Hub environment.

2.3 SAR Backscatter Principles

SAR data measures the backscatter of electromagnetic waves, offering an ideal way to distinguish between different surface types like ice and water. Additionally, this technology utilizes longer wavelengths of the electromagnetic spectrum enabling the creation of imagery irrespective of cloud cover, tree coverage, and illumination conditions. Therefore, SAR is an optimal tool for understanding the extent of ice coverage in this area of Alaska, which, during the winter months, has short daylight hours and frequent overcast weather conditions.

2.4 Data Preprocessing

Before requesting the SAR data, spatial bounds were derived from a GeoJSON file of the confluence area. To allow for temporal analysis of seasonal ice dynamics, 18 monthly time windows during the months September through May were defined across three consecutive winter seasons. Finally, in order to mitigate any noise and other various errors, radiometric calibration, speckle filtering, and geometric correction were performed and applied during the Sentinel Hub API request. To limit the ice classification to river pixels, the river network boundary was extracted through a manual digitization process using ArcGIS Pro to produce an additional GeoJSON file.

2.5 Ice Classification Method

To classify ice and open water, a threshold-based approach was applied to SAR backscatter values. After visually inspecting time slot histograms across a range of potential values, a uniform threshold of 0.45 dB was applied across all years to minimize false ice classification. The resulting ice masks for each season were then plotted in order to visualize the ice and open water pixels.

2.6 Time Series Construction

For each season, the total area of ice coverage was calculated by multiplying the number of ice-covered pixels by 1,600 m^2 for each of the 18 time slots. The pixel values were then plotted

as a time series to help visualize the variations in ice extent. The resulting time series enabled analysis of seasonal ice cover trends over the confluence across a multi-year period.

2.7 Ice Phenology Metrics

Ice dynamics were derived from the time series. Freeze-up onset was defined as the date on which the total ice area coverage exceeded 10% and peak ice date was defined as the date on which the maximum observed seasonal ice extent was achieved. The 10% threshold was chosen because all years exhibited substantial ice increases around that percentage. Breakup was defined as the date on which the first sustained ice decline below 10% occurred. The duration of ice coverage was defined as the total number of weeks between freeze-up onset and breakup for each year.

3. Results

3.1 Spatial Classification of Ice Conditions

SAR images (Figures S1-S3) were successfully classified into two conditions: ice and open water, allowing seasonal variations in ice extent to be visualized throughout the study period (Figure 1; Figure S4-S6). Ice coverage first reached the 10% freeze-up threshold between the months of October and January, depending on the study year (Table 1).

Even during the coldest winter periods, the Tanana River did not show continuous ice coverage as seen on the Yukon River (Figure 1). Possible explanations include a number of different factors including higher flow velocity, a more narrow river width, heavy glacial sediment load, and warmer groundwater from tributary inputs.

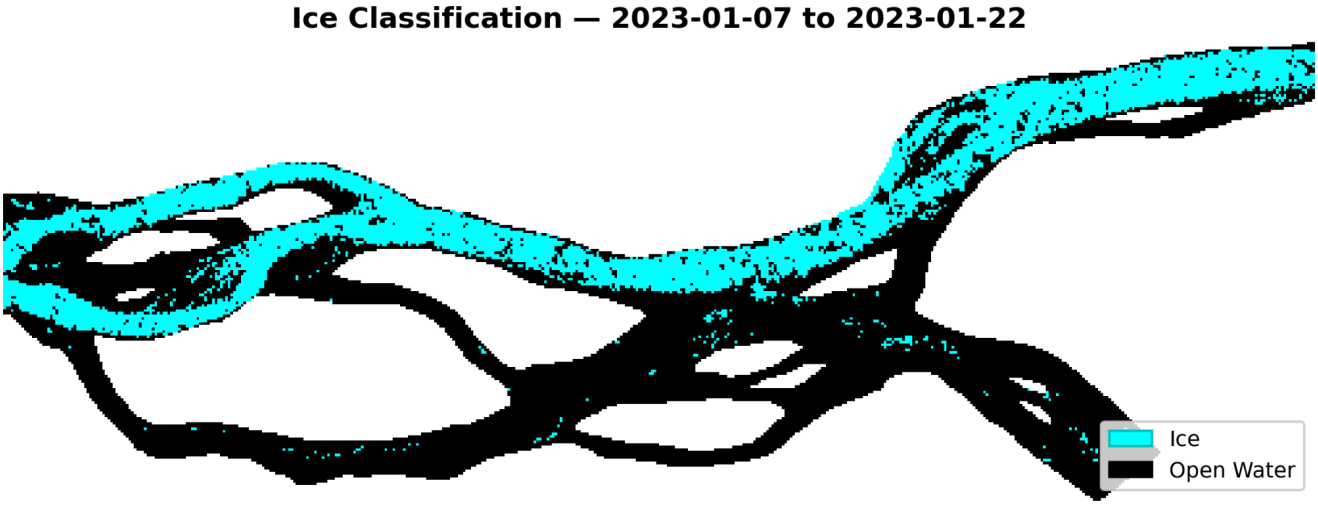

Fig 1. SAR River Ice Classification of the Yukon-Tanana River Confluence

Table 1. Winter Conditions Duration by Year

Season Years	Freeze-Up Onset	Peak Ice Conditions	Breakup	Duration of Ice Coverage
2022/2023	Mid-October	Mid-January	Late January	15 weeks
2023/2024	Late November	Mid-December & Early March	Mid-March	17 weeks
2024/2025	Early November	Mid-January	Late January	13 weeks

A VV backscatter threshold of 0.45 dB was used to evaluate whether ice and open water conditions exhibited distinguishable radar responses. Backscatter histograms were examined to evaluate radar responses throughout the seasonal cycle (Figure 2; Figure S7-S9) and a noticeable trend emerged that showed bimodal distributions throughout the winter months and more stable redistributions during transitional seasons. September and October exhibited very high pixel density at low VV values, indicating less backscatter (and less ice) during this time period. October through December showed increasing multimodal distributions with multiple local VV peaks and flattened tops, suggesting the emergence of multiple surface conditions. The winter period of December through March depicted strong secondary peaks with repeated bimodal distributions, implying that winter conditions at the confluence remained spatially mixed throughout this season. March and April showed lower VV responses with reduced secondary peaks, indicating irregular melting through intermediate states. Seasonal variability in histogram shape and spread reflect heterogeneous processes typical in freeze-up and breakup events.

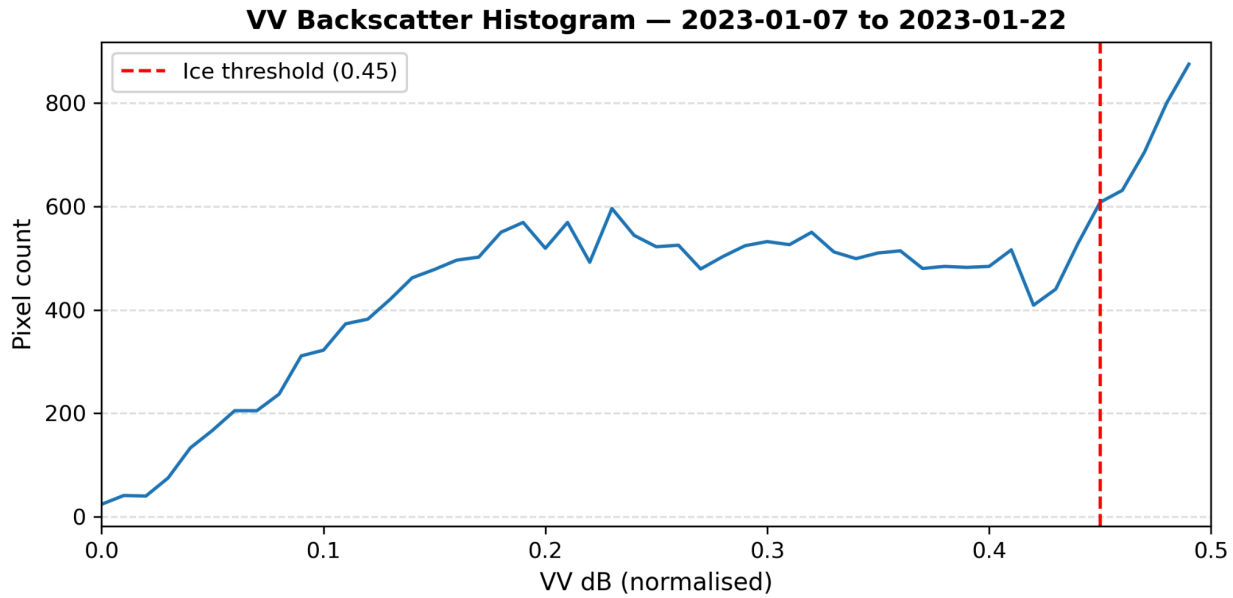

Fig 2. VV Backscatter Pixel Distribution Values

3.2 Interannual Comparison of Ice Dynamics

The ice area time series (Figure 3) revealed differences in both the timing and rate of formation and breakup of ice. During all three years, ice first surpassed the 10% freeze-up threshold in mid-October and then permanently declined below the threshold between late January and mid-March (Table 1). The peak ice area coverages for 2022/2023, 2023/2024, and 2024/2025 were 31.3%, 30.7%, 32.2% , respectively. All three seasons also exhibited short-term fluctuations in estimated ice coverage, indicating that ice conditions at the confluence can experience rapid changes throughout the winter season.

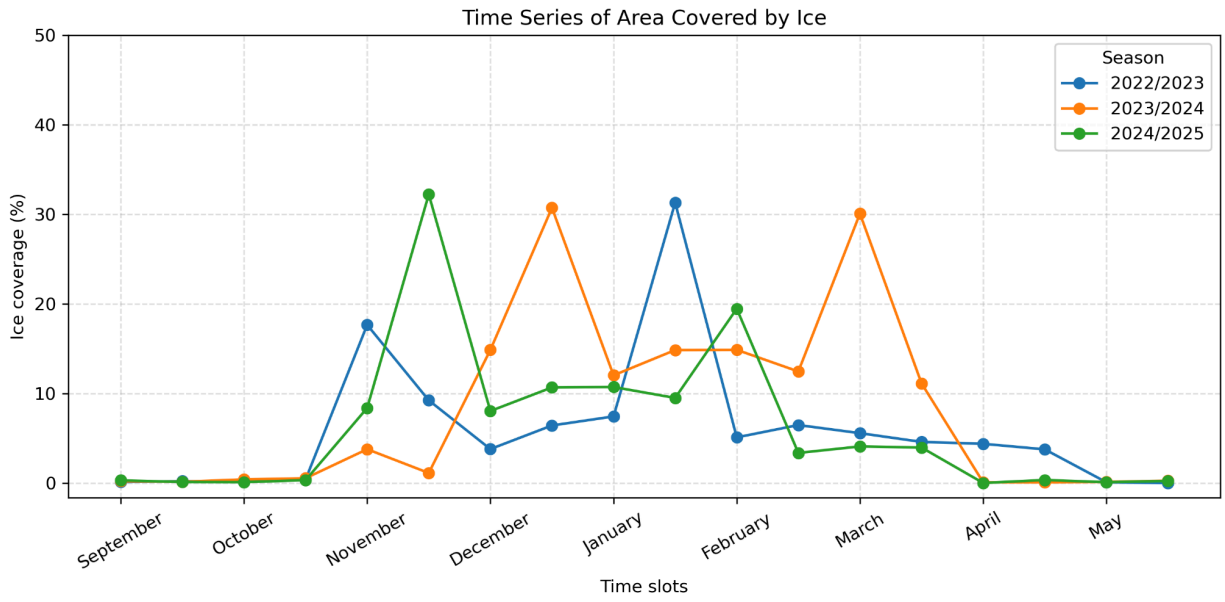

Fig 3. Interannual Ice Area Coverage Time Series

3. Discussion

Winter conditions at the Yukon-Tanana confluence across the three study years produced similar backscatter distributions and the time series graph (Figure 3) depicts an overall trend representative of expected winter season ice dynamics.

Ice formation at the Yukon-Tanana confluence was not continuous throughout the study area. Particularly, very little ice formed along the smaller channels of the Yukon River or along the Tanana River. The majority of ice formation occurred on the main channel of the Yukon River, which may reflect factors such as channel depth and width, flow rate, and water temperature.

Similar ice formation and breakup patterns across the study period occurred. Each season produced a pattern that showed an initial increase in ice extent, a stabilization of

ice coverage that lasted approximately two months, a secondary freeze-up event during the middle of the winter period, and a final break-up during the spring months. This suggests that ice formation at the Yukon-Tanana confluence is the result of a dynamic process rather than a single continuous event.

One limitation of this analysis is that the ice classification threshold was determined using a qualitative approach, which is inherently subjective. A more thorough quantitative approach, such as Otsu's thresholding, is recommended for future work in order to avoid the inherent subjectivity in this analysis's qualitative threshold estimation method. This would produce more precise results, as well as a transferable framework for additional geographic areas. Additionally, future work should focus on validating the ice classification method to assess Sentinel-1 SAR data's capability to characterize river ice dynamics.

Appendix

Appendix A – Supplemental Figures

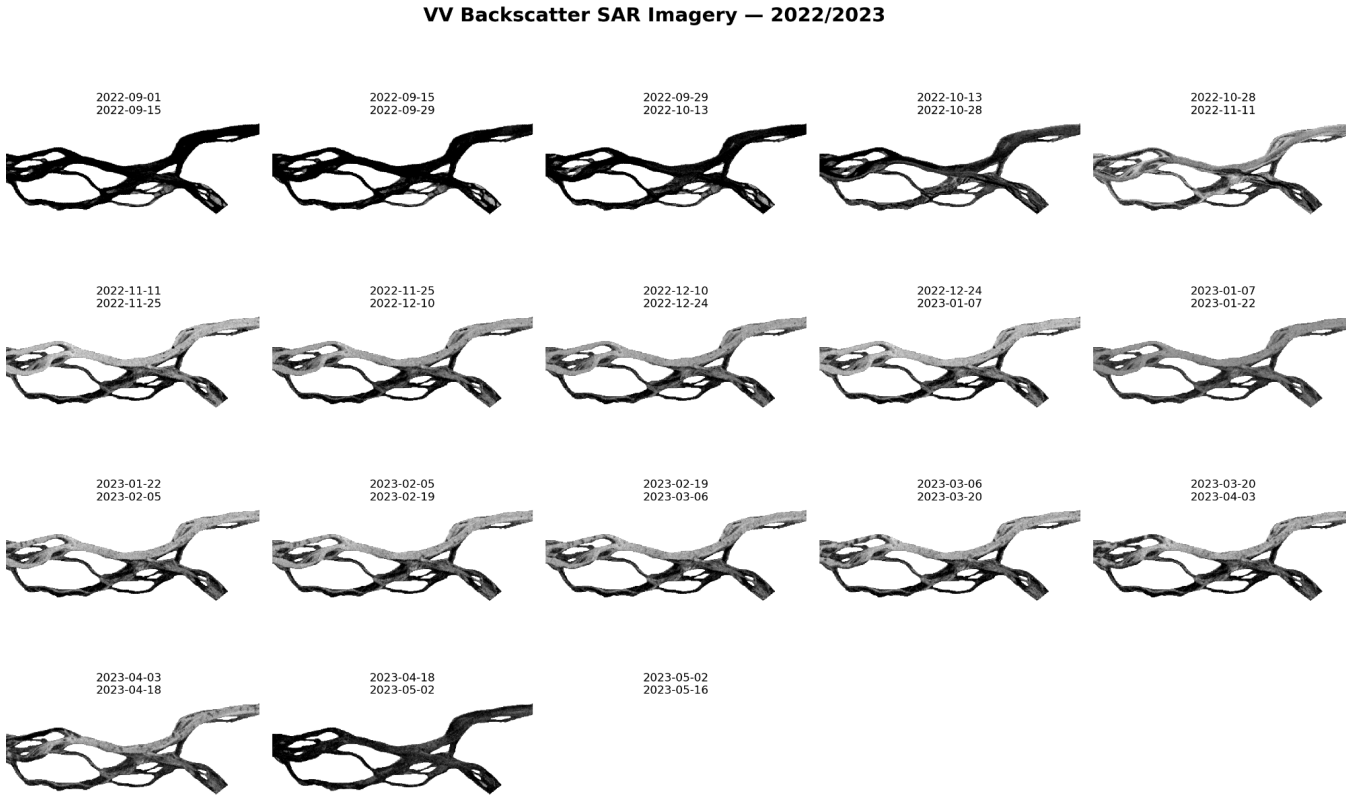

Fig S1. VV backscatter from Sentinel-1 SAR imagery over the Yukon-Tanana River Confluence in 2022/2023 winter season

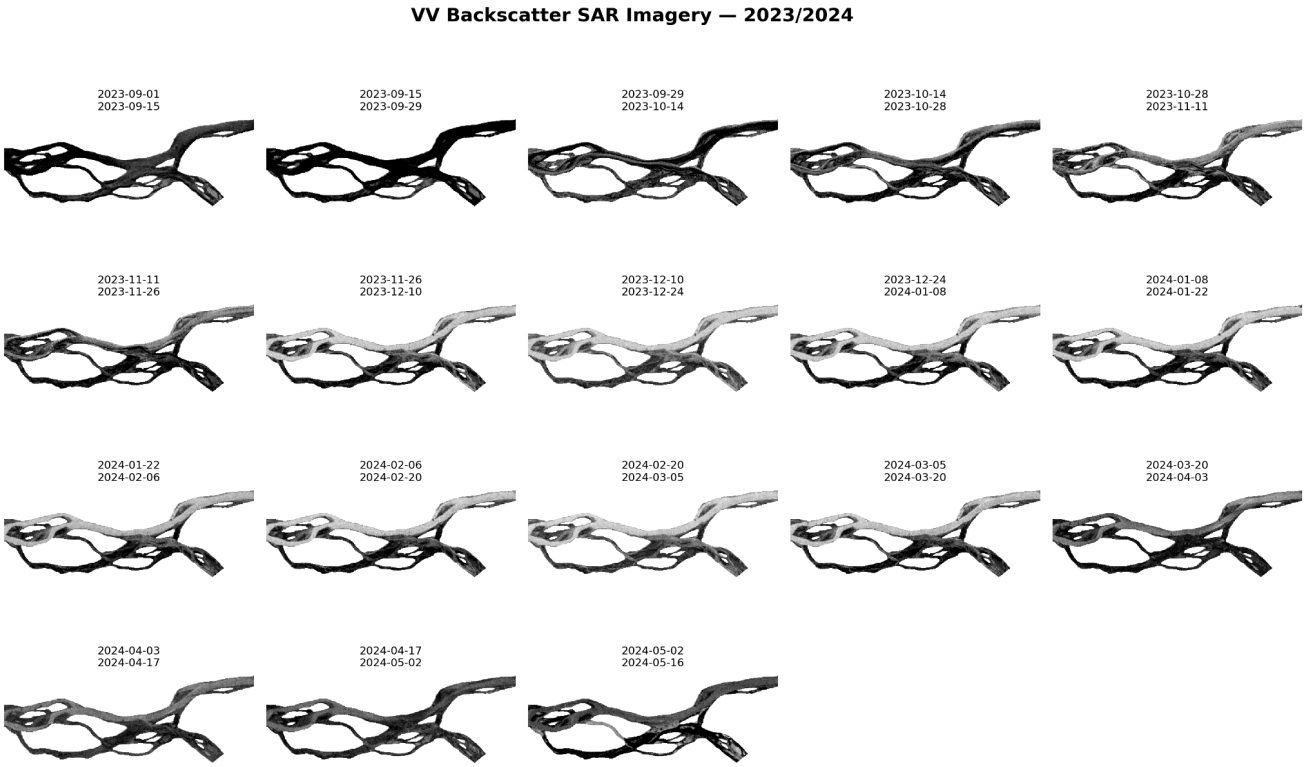

Fig S2. VV backscatter from Sentinel-1 SAR imagery over the Yukon-Tanana River Confluence in 2023/2024 winter season

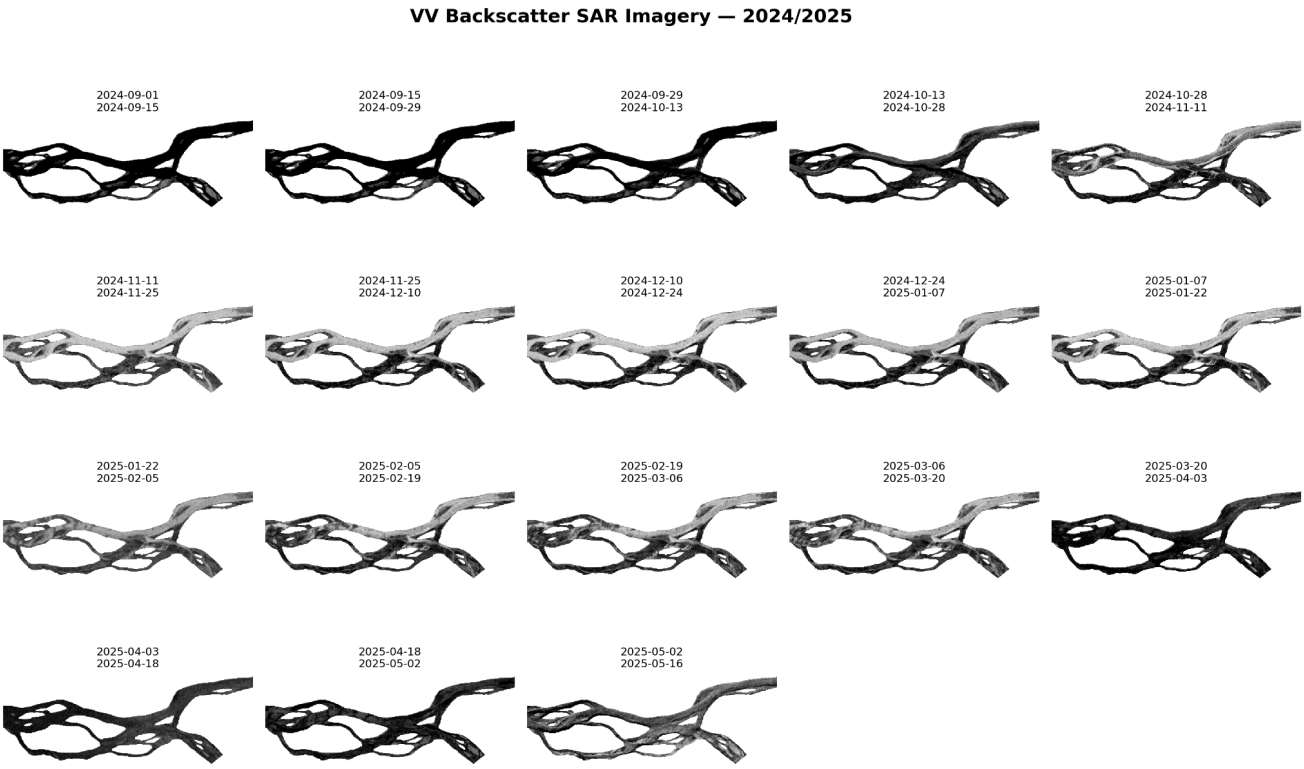

Fig S3. VV backscatter from Sentinel-1 SAR imagery over the Yukon-Tanana River Confluence in 2024/2025 winter season

Fig S4. Sentinel-1 SAR classification of ice and open water over the Yukon-Tanana River Confluence in 2022/2023 winter season

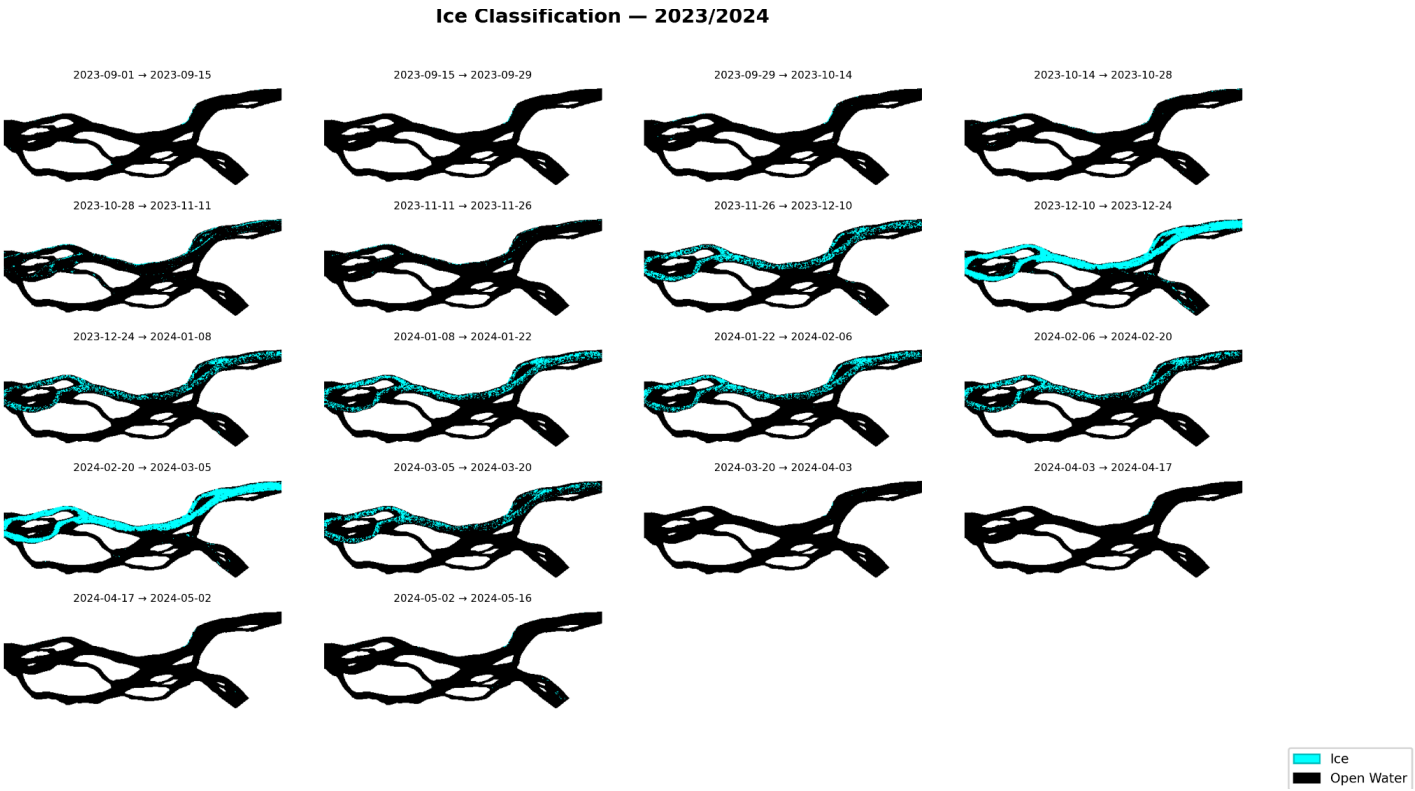

Fig S5. Sentinel-1 SAR classification of ice and open water over the Yukon-Tanana River Confluence in 2023/2024 winter season

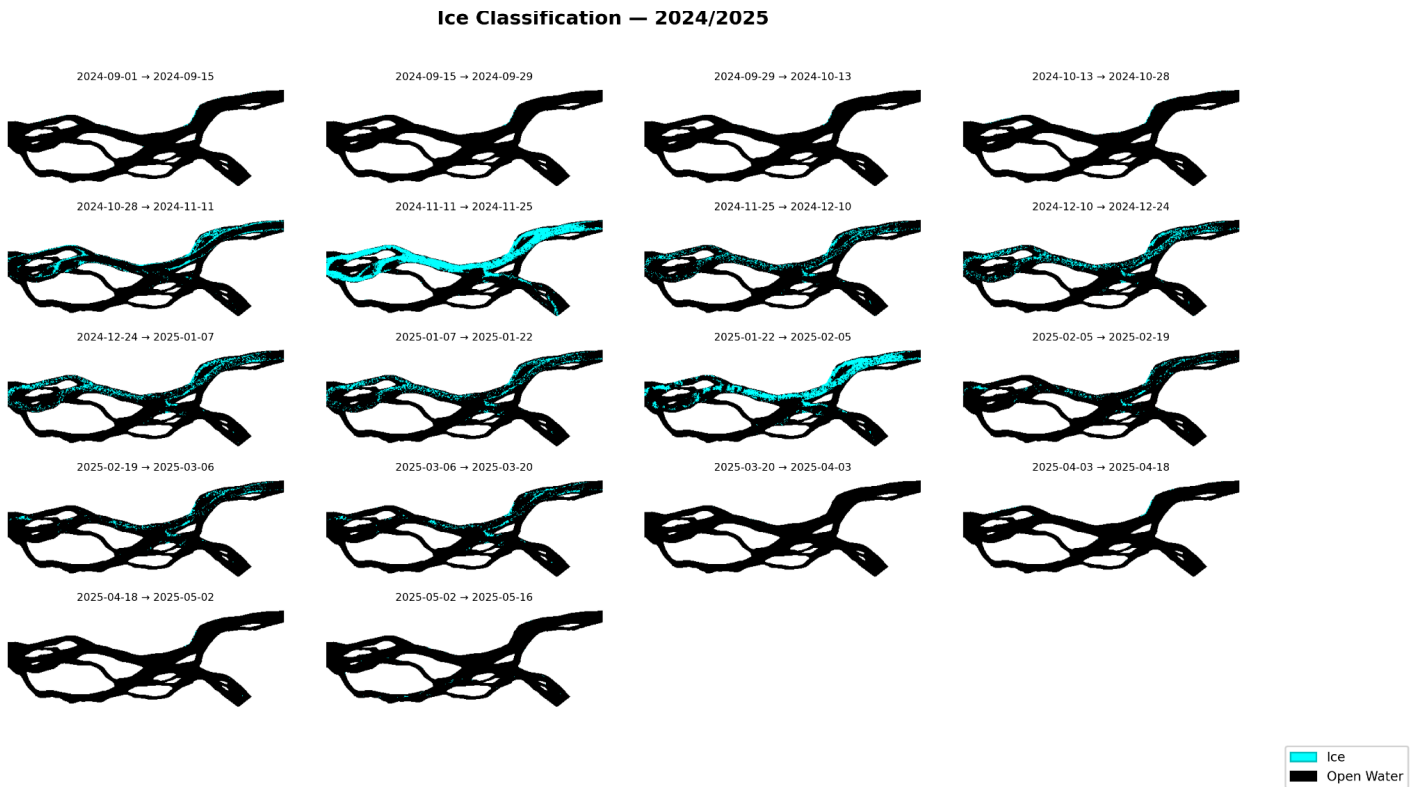

Fig S6. Sentinel-1 SAR classification of ice and not ice over the Yukon-Tanana River Confluence in 2024/2025 winter season

Appendix B – Additional Histograms

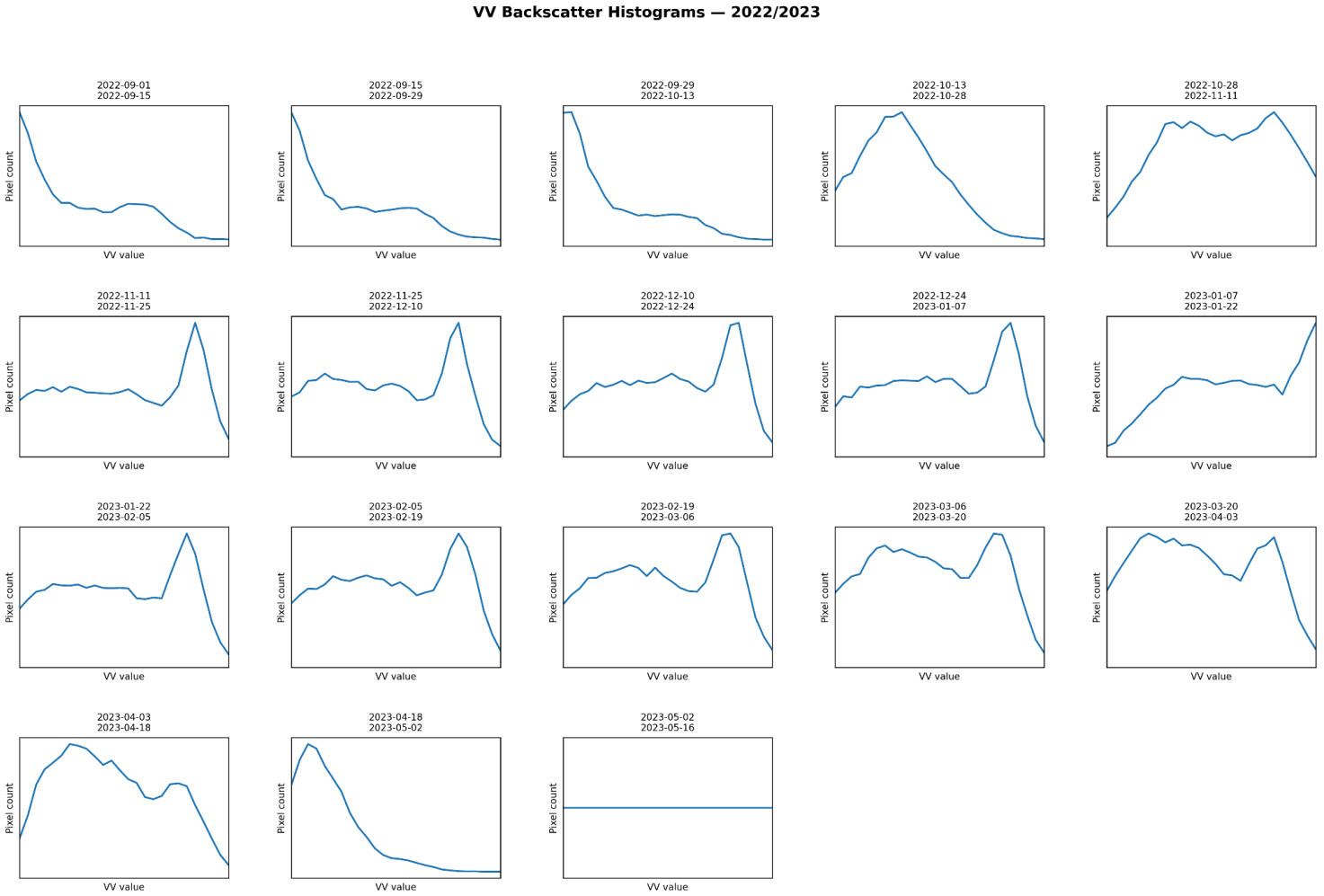

Fig S7. Sentinel-1 SAR VV backscatter histogram from the Yukon-Tanana River Confluence in 2022/2023 winter season

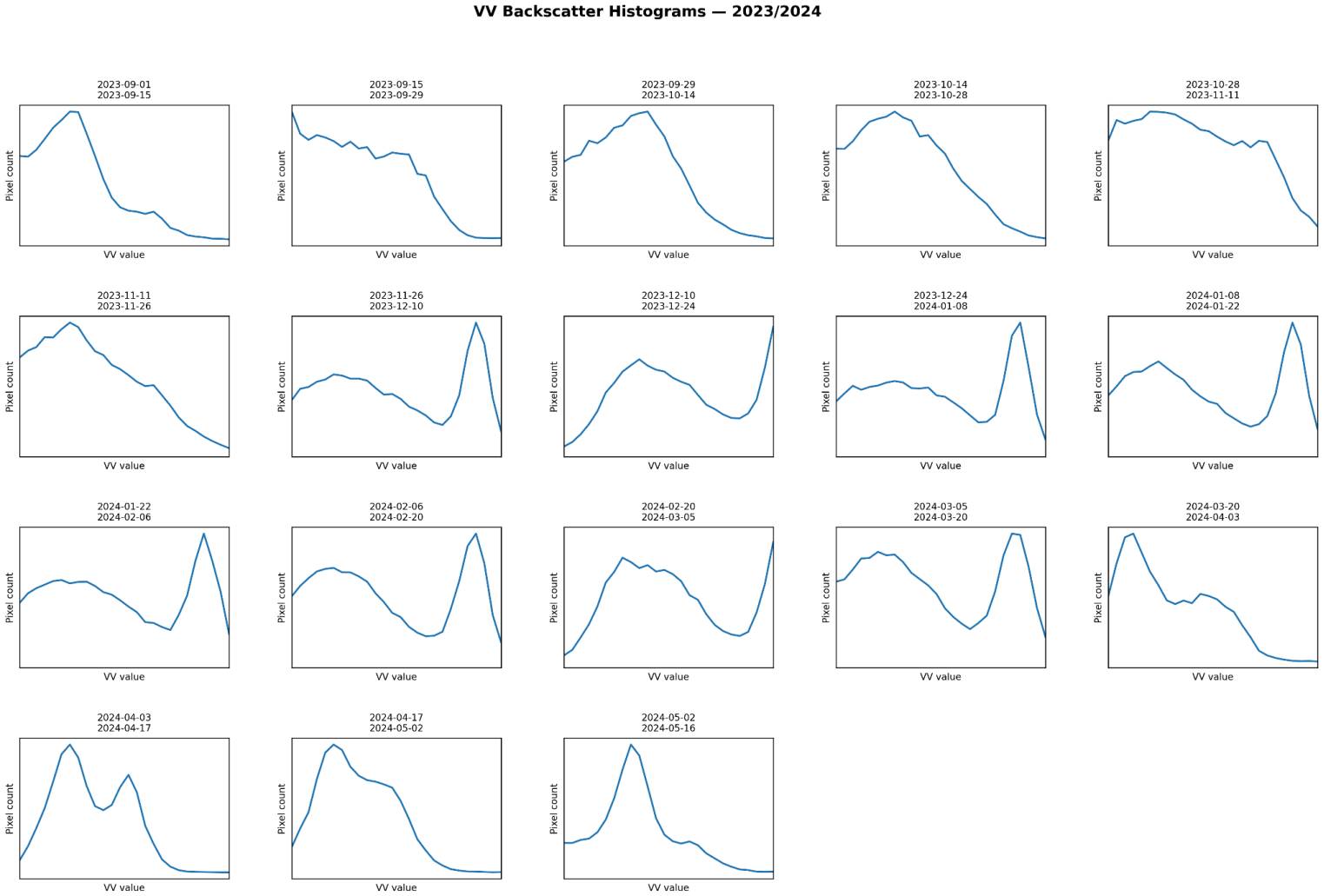

Fig S8. Sentinel-1 SAR VV backscatter histogram from the Yukon-Tanana River Confluence in 2023/2024 winter season

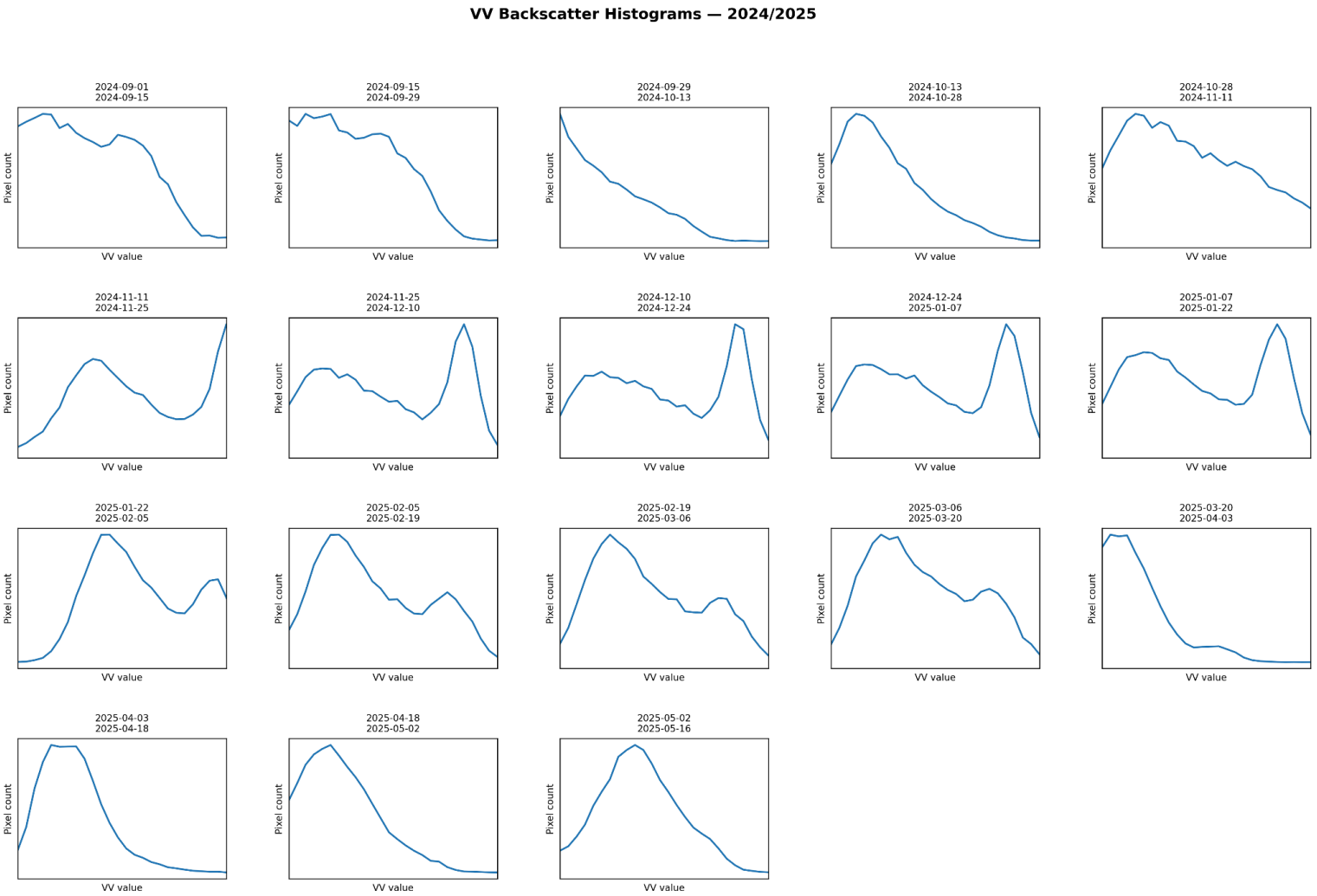

Fig S9. Sentinel-1 SAR VV backscatter histogram from the Yukon-Tanana River Confluence in 2024/2025 winter season